PERGAMON

Acta mater. Vol. 47, No. 8, pp. 2323–2330, 1999

Printed in Great Britain
PII: S1359-6454(99)00128-7
1359-6454/99 $20.00 + 0.00

UNIAXIAL STRESS–STRAIN BEHAVIOUR OF ALUMINIUM ALLOY FOAMS

K.Y.G. McCULLOUGH, N.A. FLECK and M.F. ASHBY†
Cambridge University Engineering Department, Trumpington Street, Cambridge CB2 1PZ, U.K.

(Received 13 July 1998; accepted 20 April 1999)

Abstract—The tensile and compressive stress–strain behaviour of closed cell aluminium alloy foams (trade name "Alulight") has been measured and interpreted in terms of its microstructure. It is found that the foams are anisotropic, markedly inhomogeneous and have properties close to those expected of an open cell foam. The unloading modulus and the tensile and compressive yield strengths increase non-linearly with relative density. The deformation mechanisms were analysed using image analysis software and a d.c. potential drop technique. The scatter in results is attributed to imperfections within the foam. These include non-uniform density, weak oxide interfaces, and cell faces containing voids and cracks. © *1999 Acta Metallurgica Inc. Published by Elsevier Science Ltd. All rights reserved.*

Keywords: Aluminium alloys; Foams; Deformation mechanisms

1. INTRODUCTION

Recent developments in manufacturing methods [1–4] have allowed for the development of a range of foams made from aluminium alloys. Preliminary tests (for data see Ref. [5]) have shown that for a given density the "Alulight" closed cell powder-route aluminium foams‡ are amongst the stiffest and strongest of the commercial aluminium foams. Alulight is available as sheets or cylinders with a relative density ranging from 0.1 to 0.5, and in a range of compositions. In the current study, the uniaxial properties have been measured for Al–Si casting alloys of two extreme compositions, AlMg1Si0.6 and AlMg1Si10 (wt%).

Aluminium foams have low density and are attractive materials for the cores of sandwich panels, shells and tubes. They have other desirable properties including high energy absorption [6, 7] (for packaging and crash protection), relatively low thermal conductivity [8], good electrical conductivity, high acoustic damping [9] and high fire retardance [10].

There is a developing literature on the mechanics of foams (see, for example, Gibson and Ashby [8]). Reviews of earlier work can be found in the articles by Suh and Skochdopole [11] and by Suh and Webb [12], and in the books edited by Wendle [13], Hilyard [14], Hilyard and Cunningham [15] and Banhart [16].

The aim of this study is to measure the tensile and compressive properties of Alulight closed cell foams, and to interpret these properties in terms of microstructure and cell wall properties. The effects of relative density, loading direction and silicon content on yield strength and modulus are investigated. The mechanisms of compressive deformation are analysed using a surface displacement analysis technique and a d.c. potential drop method, and the discrepancies between measured and predicted values are addressed.

1.1. Predicted properties of metallic foams

We consider a closed cell foam of density ρ^* made from solid aluminium alloy of density ρ_s. Before reporting measured values for stiffness and strength, we summarize our current theoretical understanding of the relation between the basic mechanical properties and the relative density ρ^*/ρ_s of metallic foams. Since foams can suffer large plastic strains, it is important to define stress and strain measures: we shall employ nominal measures of stress and strain throughout.

When a closed cell foam is deformed the cell edges bend, and the cell faces carry membrane stresses. The contribution from cell face stretching to the overall stiffness and strength of the foam is by a term which is linear in the relative density, ρ^*/ρ_s, while the contribution from cell edge bending is non-linear in the relative density. The result, as Gibson and Ashby [8] show, is that the yield strength of a metallic foam σ^*_{pl} in tension or compression is related to the yield strength of the cell wall material σ_y by:

$$\frac{\sigma^*_{pl}}{\sigma_y} = 0.3\phi^{3/2}\left(\frac{\rho^*}{\rho_s}\right)^{3/2} + (1-\phi)\left(\frac{\rho^*}{\rho_s}\right) \qquad (1)$$

where ϕ, the "distribution constant", is the fraction of solid in the foam which is contained in the cell

†To whom all correspondence should be addressed.
‡Supplier: Mepura Metallpulvergesellschaft m.b.H., Ranshofen, A-5282 Braunau-Ranshofen, Austria.

edges:

$$\left(\frac{\rho^*}{\rho_s}\right) \leq \phi \leq 1$$

Similarly, the unloading modulus E^* of the foam is related to the elastic modulus of the cell wall material E_s according to:

$$\frac{E^*}{E_s} = \phi^2\left(\frac{\rho^*}{\rho_s}\right)^2 + (1-\phi)\left(\frac{\rho^*}{\rho_s}\right) \quad (2)$$

Estimates for σ^*_{pl}/σ_y and E^*/E_s for the limiting case of open cell foams are obtained by setting the distribution constant $\phi = 1$; those for closed cell foams with negligible cell edges are given by $\phi = 0$.

The geometry of the cells changes with imposed strain. An extreme manifestation of this is the sharp increase in the compressive stress vs strain curve at a nominal compressive strain, termed the densification strain, which is given in Ref. [8] by:

$$\varepsilon_d \approx 1 - 1.4\left(\frac{\rho^*}{\rho_s}\right) \quad (3)$$

In order to predict accurately the properties of metallic foams it is important to have reliable data for the cell wall properties ρ_s, E_s, σ_y and ϕ. In this study we measure several of the cell wall properties independently for Alulight foams, and we compare the predictions given by equations (1)–(3) with measured data.

2. MATERIAL SPECIFICATION AND EXPERIMENTAL PROCEDURE

Flat plates of Alulight foam, of composition AlMg1Si0.6 and AlMg1Si10 (wt%), were supplied by Mepura Ltd. The plates were of dimension 145 mm by 145 mm by 9 mm, and consisted of solid skins of thickness 0.75 mm with a foam core. The plates were supplied with relative densities ranging from 0.1 to 0.5. The primary focus is the effect of foam density and composition on the tensile and compressive properties, and so the dense skins were removed by wire electro-discharge machining.

Dogbone specimens (Fig. 1) were used for tension and compression tests, and some additional compression tests were performed using smaller cuboid specimens (15 mm by 10 mm by 7.5 mm). In order to investigate the degree of anisotropy, dogbone tension specimens were cut in both the transverse and the longitudinal directions, and both dogbone and cuboid compression specimens were cut in the transverse and longitudinal directions. The Alulight plates were of insufficient thickness for dogbone specimens to be cut in the through-thickness direction: cuboid compression specimens were used.

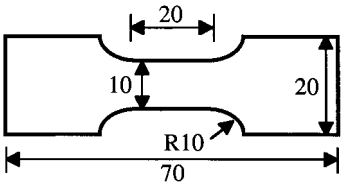

Fig. 1. Dogbone specimen. All dimensions are in mm. Specimen thickness is 7.5 mm (thickness of Alulight plate with skins removed).

The cuboid specimens were compressed to large nominal strains (up to 80%), and a linear voltage displacement transducer was used to measure the displacement of the test machine platen. A surface-mounted clip gauge was used to measure the axial strain in the gauge section of the dogbone specimens. On completion of each test on the dogbone specimens, the relative density of the gauge section was determined by cutting it out and by weighing it.

Tensile and compressive tests were performed at room temperature using a servo-hydraulic mechanical testing machine in displacement control at a rate of 0.02 mm/s. The compressive loading platens were lubricated with PTFE spray in order to minimize friction between the specimen and platens.

3. RESULTS

3.1. Typical stress–strain curves in tension and in compression

Typical stress–strain curves for the dogbone tensile specimens and the cuboid compression specimens are shown in Figs 2 and 3, respectively, for the two compositions AlMg1Si0.6 and AlMg1Si10 and for the three specimen orientations. In all cases, the density was fixed at $\rho^* = 0.65\ \mathrm{Mg/m^3}$, giving a relative density $\rho^*/\rho_s = 0.25$. The compressive yield strength σ^*_{pl} was measured at an offset plastic strain of 2%; the tensile yield strength σ^*_{UTS} was taken as the peak stress sustained by the specimen. The results are summarized in Table 1.

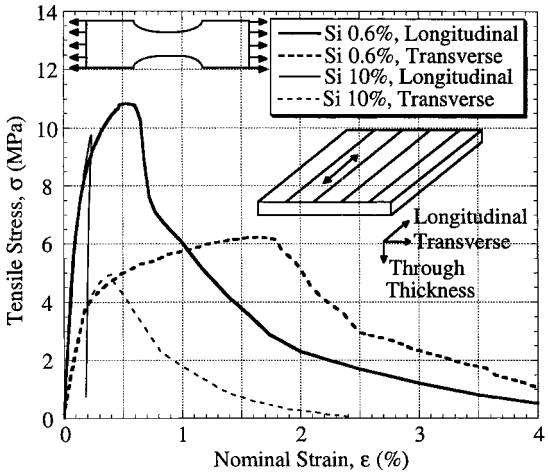

Fig. 2. Tensile stress–strain curves for AlMg1Si0.6 and AlMg1Si10, $\rho^*/\rho_s = 0.25$. Dogbone specimen geometry.

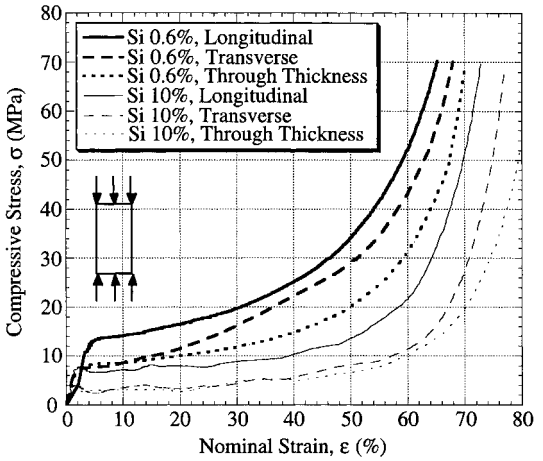

Fig. 3. Compressive stress–strain curves for AlMg1Si0.6 and AlMg1Si10, $\rho^*/\rho_s = 0.25$. Cuboid specimen geometry.

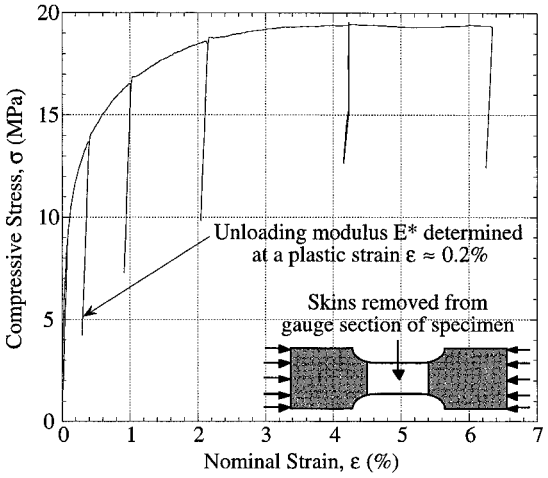

Fig. 4. Typical stress–strain curve for dogbone compressive test (AlMg1Si0.6, longitudinal orientation, $\rho^*/\rho_s = 0.28$).

The tensile and compressive yield strengths are approximately equal. The measured compressive modulus of the cuboid specimens is about one third of the tensile modulus of the dogbone specimens. This was found to be an artefact of the contact compliance between the cuboid specimen and the loading platens. To overcome this, subsequent compression tests were conducted using the dogbone geometry. A typical compressive stress–strain curve for the dogbone geometry is given in Fig. 4; the initial modulus is the same as in the tensile tests. The compressive dogbone specimens give accurate values for modulus and yield strength, but provide only limited information on the subsequent strain hardening response as the specimens buckle in compression at a nominal strain of about 6%. The unloading modulus E^* after a plastic strain of about 0.2% is significantly greater than the slope of the initial loading line. A similar discrepancy between initial and unloading moduli has been found for Alporas and Alcan metallic foams [17]. It is thought that stress concentrations within these foams lead to early yielding at isolated locations [17], resulting in an initial slope of the stress–strain curve which is considerably smaller than the true elastic modulus. The moduli reported below are those obtained from unloading tests, after a plastic strain of about 0.2% (see Fig. 4).

For any given specimen orientation, the modulus and strength are about a factor of two greater for the 0.6% Si foam than for the 10% Si foam. The densification strain is slightly sensitive to orientation and is 0.6–0.7 for the 0.6% Si foam and 0.7–0.8 for the 10% Si foam. The high silicon foam has a lower ductility than the low silicon foam, and crumbles in compression. This leads to a denser packing and to a higher densification strain in compression tests than observed for the low silicon foam. We note that the area under the nominal compressive stress vs nominal strain curve is the energy absorbed per unit initial volume. When taken to densification, the 0.6% Si foam absorbs about 130% more energy than the 10% Si foam.

The strength and the stiffness of the foam in the transverse and through-thickness directions are approximately equal to 0.75 times that in the longitudinal direction. This anisotropy is associated with the fact that the cells within the foam itself are ellipsoidal shaped: geometric constraints on the foam during manufacture cause the formation of shoebox-shaped cells which are strongest and stiffest along the longitudinal direction.

The density and elastic modulus of the cell wall materials are taken to be those of the aluminium alloys. The cell wall yield strength was measured by infiltrating the foam with epoxy, allowing microindention testing of the cell walls. For the "low silicon" AlMg1Si0.6 foam the Vickers Hardness H is 75 kgf/mm^2, corresponding to $\sigma_y \approx 250$ MPa. For

Table 1. Stress–strain results for the two compositions AlMg1Si0.6 and AlMg1Si10

Loading direction	Specimen orientation	AlMg1Si0.6		AlMg1Si10	
		σ^*_{UTS} or σ^*_{pl} (MPa)	E^* (GPa)	σ^*_{UTS} or σ^*_{pl} (MPa)	E^* (GPa)
Tension	Longitudinal	10.8	6.0	9.7	5.6
	Transverse	6.2	4.1	4.9	3.1
Compression	Longitudinal	12.7	2.1	7.7	1.1
	Transverse	7.5	1.1	4.1	0.7
	Trough-thickness	7.8	1.3	3.3	0.6

the "high silicon" AlMg1Si10 foam the Vickers Hardness is 105 kgf/mm^2, corresponding to $\sigma_y \approx 350$ MPa (assuming $\sigma_y \approx H/3$). The distribution constant, ϕ, is more difficult to determine. Quantitative metallography suggests $\phi \approx 0.7$ [18].

3.2. Variation of properties with density

A total of 44 dogbone test specimens of the AlMg1Si0.6 foam were prepared in the longitudinal and transverse directions and tested in tension and in compression. The effect of relative density upon the unloading modulus in the longitudinal direction is summarized in Fig. 5 for AlMg1Si0.6 foam; as expected, the foam stiffness increases with relative density [19, 20]. To allow for a comparison of the measured moduli with the prediction of equation (2), the foam moduli have been normalized by the cell wall modulus, $E_s = 70$ GPa, and the foam density by the cell wall density, $\rho_s = 2.67$ Mg/m^3. The curve fit through the experimental data corresponds to a fraction of cell edge material $\phi \approx 0.94$, suggesting that Alulight behaves essentially as an open cell foam.

The effect of relative density on yield strength in the longitudinal direction is summarized in Fig. 6 for AlMg1Si0.6 foam. To allow for a comparison with the prediction of equation (1), the foam yield strength has been divided by the cell wall yield strength, which has been taken as $\sigma_y = 250$ MPa, and the foam density by the cell wall density, $\rho_s = 2.67$ Mg/m^3. A best fit to equation (1) is achieved by assuming a fraction of cell edge material $\phi \approx 0.92$; this value is close to the estimate $\phi \approx 0.94$ obtained from the unloading modulus tests.

The measured unloading modulus and yield strength of the AlMg1Si0.6 foam can be summarized by simple power law fits in preference to equations (1) and (2). For the density range $\rho^*/\rho_s = 0.1$–0.4 the following approximations adequately describe the data of Figs 5 and 6:

Longitudinal direction:

$$\sigma^*_{pl} = 94\left(\frac{\rho^*}{\rho_s}\right)^{1.5}\ (\text{MPa}),\quad E^* = 90\left(\frac{\rho^*}{\rho_s}\right)^{2}\ (\text{GPa});$$

Transverse direction:

$$\sigma^*_{pl} = 70\left(\frac{\rho^*}{\rho_s}\right)^{1.5}\ (\text{MPa}),\quad E^* = 68\left(\frac{\rho^*}{\rho_s}\right)^{2}\ (\text{GPa})$$

In the above curve fits we have assumed an exponent of 1.5 for strength and 2 for modulus, as expected for open cell foams.

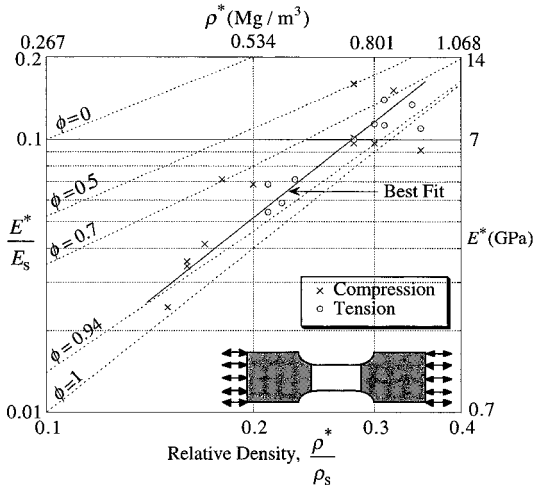

Fig. 5. Effect of relative density on unloading modulus for AlMg1Si0.6 (results for longitudinal orientation shown). Dogbone specimen geometry. The dotted lines are predictions given by equation (2). The full line is a best fit, assuming $E^*/E_s \propto (\rho^*/\rho_s)^2$.

4. DISCUSSION

It has been argued that valid tests on cellular materials require specimens with at least 10 cells along any leading dimension [17]. For both compositions the Alulight cell size varies from $l \approx 0.5$ mm for $\rho^*/\rho_s = 0.35$ to $l \approx 1.5$ mm for $\rho^*/\rho_s = 0.15$. Since the specimen thickness is 7.5 mm, the number of cells in the thickness direction varies from 5 to 15. To check that specimens with 5 cells in the thickness direction give accurate results additional cuboid compression specimens of $\rho^*/\rho_s = 0.35$ and cell size 0.5 mm were manufactured with a thickness of 5 cell sizes: these specimens gave identical results to those for specimens of thickness 15 times the cell size.

There exists at least three types of imperfection which degrade the stiffness and strength of Alulight [17, 21, 22]; cell edge curvature, large Plateau borders (material concentrated at cell nodes rather than at cell edges), and non-uniform foam density (redundant solid material and large isolated voids). If a specimen comes from a poorly processed plate, it contains voids of up to 4 cells in diameter. With a cross-section of approximately 10 by 8 cells this causes a significant reduction in effective cross-sectional area. The manufacturing method also creates weak oxide interfaces within the foam and regions of low density foam adjacent to these interfaces [20].

4.1. Weibull parameters

The test results display a significant amount of experimental scatter, see for example Figs 5 and 6. This scatter is caused by the imperfections in the foam, and in particular by the regions of high porosity. The yield strength scatter can be characterized in both tension and compression by an equation with the form of that associated with a Weibull distribution of strength [23]

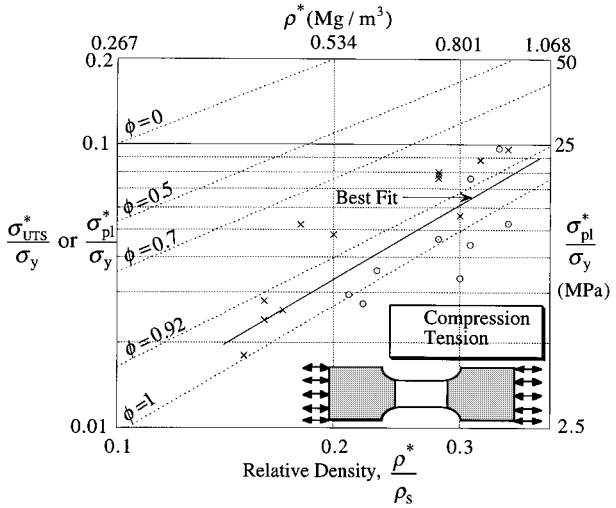

Fig. 6. Effect of relative density on yield strength for AlMg1Si0.6 (results for longitudinal orientation shown). Dogbone specimen geometry. The dotted lines are predictions given by equation (1). The full line is a best fit, assuming $\sigma^*_{pl}/\sigma_y \propto (\rho^*/\rho_s)^2$.

$$\ln P_s(V) = -\frac{V}{V_0}\left(\frac{\sigma}{\sigma_0}\right)^m \qquad (4)$$

where $P_s(V)$ is the survival probability of a specimen of volume V under stress σ, and m is the Weibull modulus. The reference stress σ_0 is the value of stress giving a survival probability of $e^{-1} = 0.32$ for a specimen of volume V_0. The sample size for each of the configurations discussed below was 11 specimens.

For the AlMg1Si0.6 foam the longitudinal compressive strength has a Weibull modulus m of 12, and the longitudinal tensile strength has a modulus

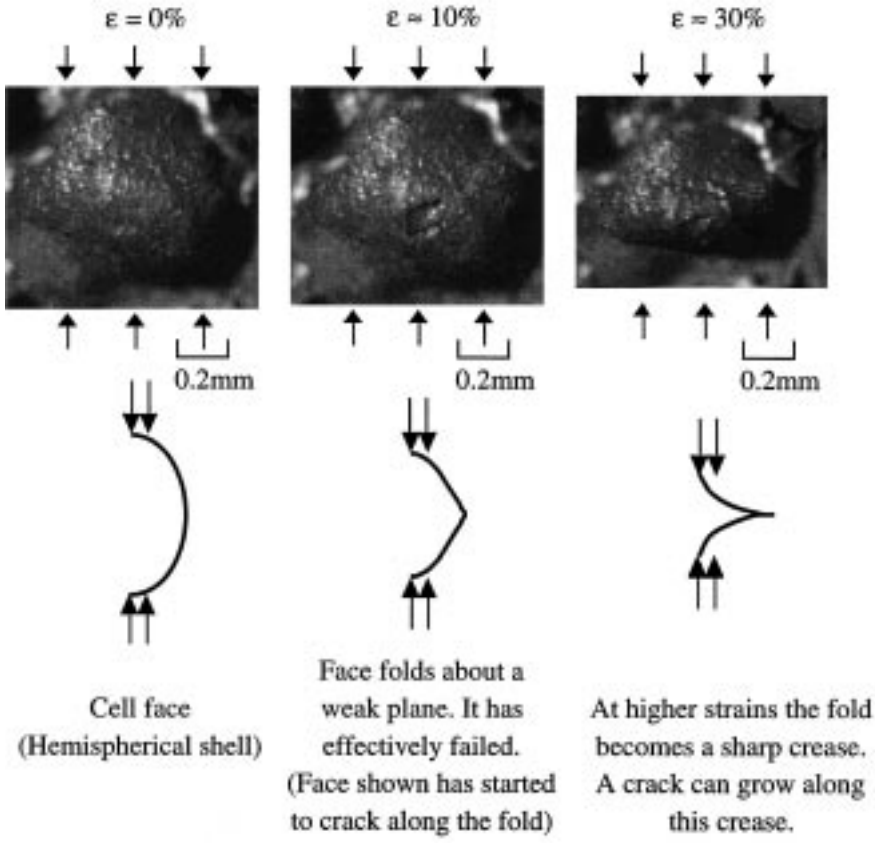

Fig. 7. Micrographs of a compression test to show failure of cell faces (AlMg1Si0.6, transverse orientation, $\rho^*/\rho_s = 0.22$). Cuboid specimen geometry.

of 10. In the transverse direction the Weibull compressive strength modulus equals 12, but the tensile strength modulus equals only 7. This dispersion in transverse tensile strength is associated with the fact that the specimens contain weak oxide interfaces with unit normal along the transverse direction.

These low values of Weibull modulus are comparable to those observed for engineering ceramics, and are much less than those typical of fully dense metallic alloys. Further developments in processing are desirable in order to achieve more uniform microstructures and more consistent properties for metallic foams such as Alulight.

4.2. Properties and structure

When Alulight in the as-received state is examined under a scanning electron microscope (SEM), hairline cracks and voids are evident in approximately a third of the cell faces, explaining why the foam sinks when placed in water. The cell faces behave as weak shell-like structures and fold at a nominal compressive strain $\varepsilon \approx 10\%$, see Fig. 7. As the nominal strain level is increased, cracks grow along the plastic hinges in the cell faces. However, by this point the fold has already degraded the contribution of the face to strength and stiffness, and so the local cracking has little effect on foam stiffness or strength. The overall behaviour of the foam is therefore dominated by bending of the cell edges, that is to say the foam behaves in an open cell manner. The curve-fits for the yield strength and modulus results (Figs 5 and 6), suggesting an effective fraction of cell edge material of $\phi = 0.92$–0.94, are consistent with this observation.

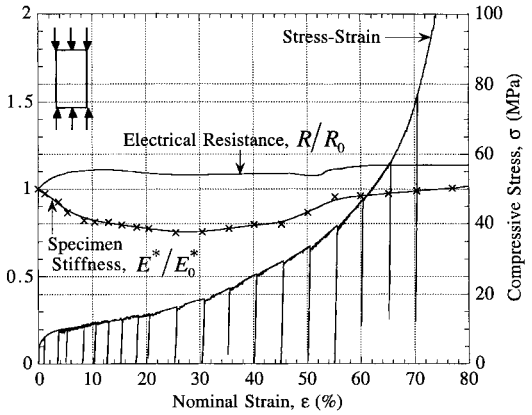

Fig. 8. Variation of stiffness and electrical resistance with nominal strain (AlMg1Si0.6, transverse orientation, $\rho^*/\rho_s = 0.29$). Cuboid specimen geometry.

4.3. Deformation mechanisms

In order to probe the deformation response of the foam in compression, the variations in unloading modulus and electrical resistance with strain were examined in a number of compression tests on cuboid specimens of AlMg1Si0.6 (see Fig. 8). Electrical resistance was measured using a d.c. potential drop technique: a constant 3 A current was passed through the specimen and the voltage drop across the specimen was monitored. The electrical resistance increases with crack density within the foam, but is almost independent of plastic deformation. The initial electrical resistivity of the

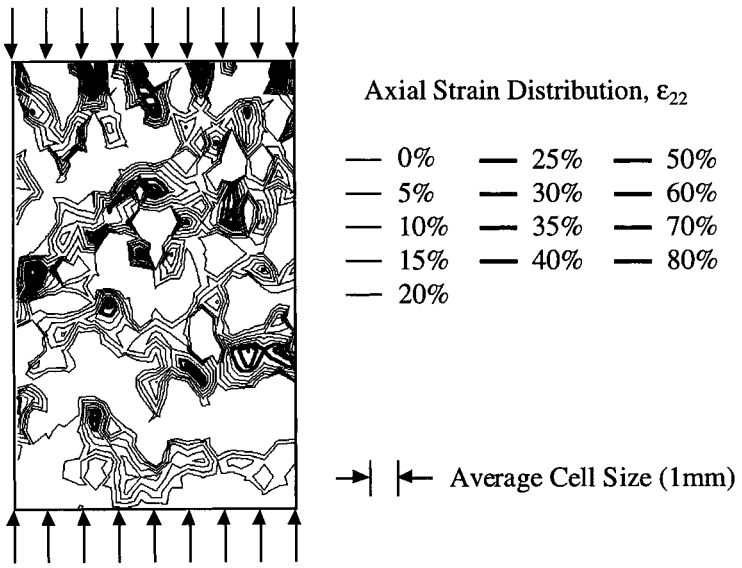

Fig. 9. Axial strain distribution under nominal compressive strain $\varepsilon = 20\%$ (AlMg1Si0.6, transverse orientation, $\rho^*/\rho_s = 0.25$, contours with $\varepsilon_{22} > 20\%$ shown in bold). Cuboid specimen geometry.

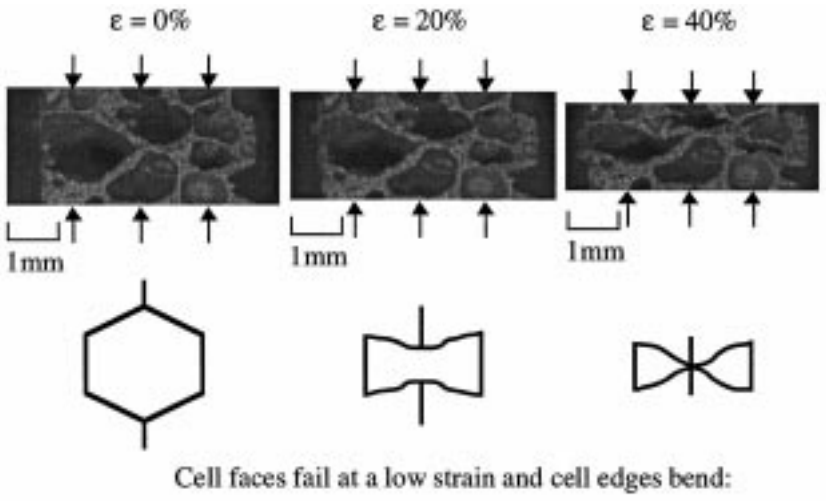

Fig. 10. Micrographs of a compression test to illustrate cell edge bending (AlMg1Si0.6, transverse orientation, $\rho^*/\rho_s = 0.18$). Cuboid specimen geometry.

AlMg1Si0.6 Alulight is approximately 8 mΩ/m for $\rho^*/\rho_s = 0.29$.

A typical plot of the evolution of unloading modulus and electrical resistance with compressive strain is shown in Fig. 8. These plots suggest that the yield strength and modulus are dominated by the contribution from cell wall bending, by the following argument. If the modulus of the foam depends on cell face stretching, then as the strain increased and these membranes rupture the modulus would be expected to drop significantly. We note from Fig. 8 that the modulus drops by only 10% and the electrical resistance increases by about 10% when the compressive strain is increased to 10%. SEM examination reveals that most of the cell faces have already failed at this strain level. With additional straining there is little further cracking of the cell faces and cell edges: the electrical resistance remains approximately constant. The drop and subsequent rise in unloading modulus with additional strain is associated with changes in cell geometry with deformation.

A transverse specimen of Alulight was compressed and examined using Instron Surface Displacement Analysis (''speckle'') software [24]. The software captures images of the surface of the specimen while it is deforming under load, and then compares and analyses pairs of these images. The in-plane surface displacement field is mapped and converted into strain contours. A plot of the axial strain distribution (ε_{22}) at a nominal strain of 20% (compared to the unstrained state) is shown in Fig. 9. It shows an apparently random distribution of strain, wherein some areas of foam are apparently uncrushed whilst others suffer large local strains (for clarity the contours for $\varepsilon_{22} > 20\%$ have been highlighted).

The clusters of high strain contours in Fig. 9 represent the deformation of individual cells. An individual weak cell is unable to crush in an isolated manner as it is constrained by an elastic cage of neighbouring cells; rather it is the initiation point for a crush band that propagates through the foam. It is conjectured that crushing is by the transverse propagation of a crush band, analogous to a Mode I crack. Figure 10 shows the mechanism of individual cell crushing: it is by the bending of cell edges.

After a row of cells has crushed, the band locks-up, and deformation proceeds elsewhere at a new crush band. Thus, the macroscopic strain is due to the sequential crushing of individual rows of cells; the spatial scatter in crush strength is such that successive crushing does not occur at adjacent rows of cells. As a consequence of this scatter in crush strength the foam exhibits considerable work hardening. This argument suggests that the greater the dispersion in crush strength the greater is the work hardening rate of the foam.

In tension it appears that once the first weak plane has failed the specimen fractures—thus only one ''weak link'' needs to be broken to cause tensile failure. The tensile failure strain is only $\varepsilon \approx 2$–4%.

5. CONCLUSIONS

In tension Alulight behaves in a semi-brittle fashion, whereas in compression a ductile behaviour is observed. Yield strength and unloading modulus are equal in tension and compression, and increase non-linearly with relative density. A low silicon content produces a stiffer and stronger foam. In both tension and compression the foam yields almost immediately upon loading; this results in an unloading modulus significantly greater than the slope of the initial loading line.

Alulight is anisotropic: its yield strength and unloading modulus in the transverse and through-thickness directions are approximately 0.75 times

those in the longitudinal direction. It is markedly inhomogeneous; in particular, the manufacturing process creates weak oxide interfaces with regions of low density foam adjacent to these interfaces. Furthermore, its cell faces are highly defective and relatively thin; they fail at a low applied strain, and consequently Alulight has properties close to those of an open cell foam. The imperfections in the foam cause considerable scatter in the test results.

Acknowledgements—The authors are grateful to DARPA/ONR for their financial support through MURI grant number N00014-1-96-1028 on the Ultralight Metal Structures project at Harvard University, to T.J. Lu for many constructive comments, and to A. Heaver and S. Marshall for their technical assistance.

REFERENCES

1. Baumeister, J. and Schrader, J., German Patent no. DE 41 01 630, 1991.
2. Davies, G.J. and Zhen, S.J., *Mater. Sci.*, 1983, **18**, 1899.
3. Akiyama, S. *et al.*, U.S. Patent no. 4,713,277, 1987.
4. Sang, H., U.S. Patent no. 5,334,236, 1994.
5. Ashby, M.F., *Metal Foams and Honeycombs Database*. Granta Design, Cambridge, U.K., 1996.
6. Thornton, P.H. and Magee, C.L., *Metall. Trans.*, 1975, **6A**, 1253.
7. Niebylyski, L.M. and Fanning, R.J., *SAE Trans.*, 1973, **81**, 1676.
8. Gibson, L.J. and Ashby, M.F., *Cellular Solids: Structures and Properties*, 2nd edn. Cambridge University Press, Cambridge, 1997.
9. Lu, T.J., Stone, H.A. and Ashby, M.F., *Acta mater.*, 1998, **46**, 3619.
10. Koch, A. *et al.*, in *Proc. 4th Int. Conf. on Aluminium Alloys*, Atlanta, GA, 1994, Georgia Institute of Technology, ed. T. H. Sanders Jr, pp. 387–394.
11. Suh, K.W. and Skochdopole, R.E., *Foamed Plastics, Encyclopedia of Chemical Technology*, Vol. 2, 3rd edn. Wiley, New York, 1980.
12. Suh, K.W. and Webb, D.D., *Cellular Materials, Encyclopedia of Polymer Science*, Vol. 2, 3rd edn. Wiley, New York, 1985.
13. Wendle, B.C., *Engineering Guide to Structural Foams*. Technomic Publishing Co. Westport, CT, U.S.A., 1976.
14. Hilyard, N.C., *Mechanics of Cellular Plastics*. Applied Science, London, U.K., 1982.
15. Hilyard, N.C. and Cunningham, A., *Low Density Cellular Plastics: Physical Basis of Behaviour*. Chapman and Hall, London, 1994.
16. Banhart, J. (ed.), *Metallschaume*. MIT, Bremen, 1997.
17. Sugimura, Y. *et al.*, *Acta mater.*, 1997, **45**, 5245.
18. Murphy, A.M., unpublished research, 1998.
19. Beals, J. and Thompson, M., *J. Mater. Sci.*, 1997, **32**, 3595.
20. Krizst, B., written communication, 1997.
21. Grenestedt, J.L., *J. Mech. Phys. Solids*, 1998, **46**, 29.
22. Simone, A.E. and Gibson, L.J., *Acta mater.*, 1998, **46**, 2139.
23. Ashby, M.F. and Jones, D.R.H., *Engineering Materials*, Vol. 2. Pergamon Press, Oxford, 1986.
24. Bastawros, A. and McManius, R., *Experimental Techniques*, 1998, **22**, 35.